Supporting material: Modelling spatially regulated β-catenin dynamics and invasion in intestinal crypts

Philip J. Murray
Jun-Won Kang
Gary R. Mirams
Sung-Young Shin
Helen M. Byrne
Philip K. Maini
Kwang-Hyun Cho

Derivation of the single crypt model

In this section we explain how the fluxes and production rate are modelled, prescribe supplementary conditions, describe how the numerical solution is computed and discuss the validity of the model assumptions.

$J_y(y, s, \tau)$: Crypt Dynamics Model

Applying conservation of cell number in (y, s, τ) space, we obtain the conservation equation

$$\frac{\partial p(y,s,\tau)}{\partial \tau} + \frac{\partial J_y(y,s,\tau)}{\partial y} + \frac{\partial J_s(y,s,\tau)}{\partial s} = r(p, y, s, \tau), \tag{S1}$$

where $J_y(y, s, \tau)$ is the physical cell flux along the crypt axis, $J_s(y, s, \tau)$ is the cell flux resulting from subcellular β-catenin dynamics and r is the net cell production rate (see schematic diagram in Fig. S1). The structure of Eq. (S1) is similar to age- or size-structured models (e.g. 1, 2); the main difference is that we consider a cell population structured according to intracellular β-catenin concentration rather than cell age or size.

Before continuing it is convenient to introduce the spatial cell number density, $q(y, \tau)$, which is defined as follows:

$$q(y,\tau) = \int_0^\infty p(y,s,\tau)ds. \tag{S2}$$

Using this quantity we define the cell flux

$$J_y(y,s,\tau) = -\frac{D(q)}{q}\frac{\partial q}{\partial y}p(y,s,\tau), \tag{S3}$$

where $D(q) = \frac{\alpha}{q^2}$ and α is the cell spring constant/viscosity ratio. This choice for the flux can be rationalised by assuming that J_y is convective (i.e. $J_y = vp$) with v chosen to be the cell velocity field of a one-dimensional chain of cells connected by overdamped linear springs (3)

$$v(q, \frac{\partial q}{\partial y}) = -\frac{D(q)}{q}\frac{\partial q}{\partial y}. \tag{S4}$$

Hence the flux defined in Eq. (S3) represents a continuum one-dimensional approximation of the mechanics system considered by Meineke et al. (4) and van Leeuwen et al. (5).

$J_s(y, s, \tau)$: Wnt Signalling Model

The canonical Wnt signalling pathway couples cell positional information to cell proliferation and differentiation via β-catenin, a key downstream effector that regulates the transcription of hundreds of genes related to cell proliferation. Lee et al. (6) have developed an ODE model of this pathway. While Lee *et al.*'s original model consisted

of 15 ODEs, Mirams et al. (7) have recently shown, using asymptotic analysis, that the system dynamics simplify into activity upon a short (fast), an intermediate, and a long (slow) timescale. They observed that β-catenin dynamics occur solely on the long timescale, allowing them to propose a highly simplified single-ODE model which retains the cytoplasmic β-catenin dynamics in response to Wnt signalling:

$$\frac{ds}{d\tau} = g(W(y), s), \tag{S5}$$

where

$$g(W(y), s) = a - \left(\left(\frac{W(y)+b}{cW(y).+d}\right)\left(\frac{e}{e+s}\right)+f\right)s. \tag{S6}$$

Here $W(y)$ represents the external concentration of Wnt which takes dimensionless values in the range $0 < W(y) < 1$; a and f are rate constants for production of β-catenin and degradation of β-catenin respectively (in a natural turnover, destruction-complex independent manner). The remaining terms denote the destruction-complex-dependent degradation: b is a dimensionless parameter, representing the activity of the destruction complex in the absence of Wnt; c and d are timescales dictating how the rate of β-catenin degradation increases and saturates in the absence of Wnt; and e is a Michaelis-Menten β-catenin association constant. The parameter values are presented in Table 1 of the main text. The steady-state of Eq. (S5) is plotted in Fig. S2. In Mirams et al. (7) the parameters a–f are given as groups of the original Lee et al. (6) parameters, so that in their original notation:

$$\begin{aligned}
a &= v_{12} \\
b &= \frac{k_2}{k_1}, \\
c &= \Big(k_1k_3Dsh^0 + k_1k_{-6}\Big)\Big(k_5k_{15}K_7K_8\Big)\Big/\Big(k_1k_4k_6k_9v_{14}GSK^0APC^0\Big), \\
d &= \Big(k_2k_5k_{-6}k_{15}K_7K_8\Big)\Big/\Big(k_1k_4k_6k_9v_{14}GSK^0APC^0\Big), \\
e &= K_{17}, \\
f &= k_{13}.
\end{aligned}$$

Cho et al. (8) have considered how different truncation mutations of the APC gene that modify APC-mediated β-catenin destruction can be captured in the Lee et al. (6) Wnt signalling model, suggesting modified values for K_7 and K_8 for various truncations (8). Upon substitution of these 'mutant' values into the above expressions, we find parameter changes are manifest in the reduced Mirams et al. (7) model through simple increases in the parameters c and d (as shown in Table 3 in the main text) for increasingly severe truncation mutations.

In order to capture Wnt regulation of cell proliferation via β-catenin, we assume that cell flux along the s axis, J_s, (treating y as constant) is comprised of two components: a convective term originating from the subcellular β-catenin dynamics captured by Eq. (S6) and a diffusive term representing subcellular variability at the cell population scale. The cell flux is therefore given by

$$J_s(y, s, \tau) = g(y, s)p(y, s, \tau) - D_s\frac{\partial p}{\partial s}, \tag{S7}$$

where D_s is a measure of the noise strength.

Net cell proliferation is modelled via $r(p, y, s, \tau)$, the term on the right-hand-side of Eq. (S1). As β-catenin is a transcription factor which regulates a large number of genes related to cell proliferation, we assume that cells can divide only if their β-catenin concentration exceeds the threshold s^* and that the cells in the proliferative region have a proliferation rate, $\rho(1 - \frac{q}{K})$, such that cell proliferation occurs only if the local cell density is less than the carrying capacity, K. Hence the cell production rate is given by

$$r(p, y, s, \tau) = \rho p(y, s, \tau)(1 - \frac{q}{K})H(s - s^*), \tag{S8}$$

where $H(.)$ denotes a Heaviside function. We remark that for simplicity we do not explicitly distinguish between the proliferation rates of stem and transit cells: the differences in proliferative activity between these two populations is absorbed in the averaged cell proliferation rate, ρ. We also assume that cell apoptosis is negligible along the crypt axis and that all cell removal occurs via cell shedding at the top of the crypt.

Substituting for the flux terms J_y, J_s and the net cell production rate, r, from Eqs. (S3), (S7) and (S8) in Eq. (S1), we arrive at the following nonlinear integro-differential equation given by

$$\begin{aligned}\frac{\partial p(y, s, \tau)}{\partial \tau} = & \frac{\partial}{\partial y}\left(\frac{D(q)}{q}\frac{\partial q}{\partial y}p(y, s, \tau)\right) \\ & + \frac{\partial}{\partial s}\left[-\left(a - \left(\left(\frac{W + b}{cW(y) + d}\right)\left(\frac{e}{e + s}\right) + f\right)s\right)p(y, s, \tau) + D_s\frac{\partial p}{\partial s}\right] \\ & + \rho p(y, s, \tau)(1 - \frac{q}{K})H(s - s^*).\end{aligned} \tag{S9}$$

As discussed in the Main Text, we close Eq. (S9) by imposing the following boundary and initial conditions:

$$W(y) = e^{-\frac{y}{\lambda}}, \tag{S10}$$

$$\frac{\partial q}{\partial y}_{y=0} = 0; \tag{S11}$$

$$q(L, \tau) = \frac{1}{l}; \tag{S12}$$

$$J_s(y, 0, \tau) = 0; \qquad J_s(y, \infty, \tau) = 0; \tag{S13}$$

$$p(y, s, 0) = p_0(y, s). \tag{S14}$$

Numerical solution

In order to solve Eqs. (S9) - (S14) numerically, we discretise using a regular mesh with $\Delta y = \frac{L}{N_y - 1}$ and $\Delta s = \frac{s_{max}}{N_s - 1}$ so that the y and s axes are discretised using N_y and N_s equally spaced nodes, respectively. At each time step, $q(y, \tau)$ is approximated using Simpson's rule while the partial derivatives that appear in Eq. (S9) are approximated using first order finite differences. The method of lines is then used to compute the

time derivative and the resulting system of nonlinear ODEs is solved using the Matlab stiff-ODE solver 'ode15s' .

Additional numerical results

While it is impossible to conduct an exhaustive search of the parameter space of this model, here we present further simulation results in order to illustrate how model behaviour depends on parameter values. In Fig. S3 average β-catenin concentrations are plotted against crypt height for the increasingly truncated APC mutations introduced in the Main Text. In Figs. S4-S6 we present numerical solutions to Eqs. (S9) - (S14) in different regions of parameter space. In Fig. S4 the effective rate of β-catenin activation has been increased by a factor of two. This results in a shift in the steady-state β-catenin concentrations along the crypt axis. Consequently, cell proliferation occurs throughout the crypt as the β-catenin division threshold is exceeded. In Fig. S5 the cell proliferation rate ρ has been increased from 0.10 to 0.11. The β-catenin dynamics remain close to the 'wild-type' case presented in Fig. 2 of the Main Text but the increased cell proliferation rate results in larger cell densities at the bottom of the crypt. In Fig. S6 the diffusion coefficient, D_s, which represents noise in the β-catenin dynamics, has been increased by a factor of two and the distribution of cells about the steady-state β-catenin concentration broadens.

Comparison with experimental data

In Table S1 numerical results from Eqs. (S9) - (S14) are compared with data from murine small intestinal crypts (9). In order to calculate the total cell number and proliferative fraction in the crypt, we assume that there are 16 cells along the crypt circumference (9). Since our model does not account for the hemispherical shaped crypt bottom, we expect the numerical results to overestimate the total cell number and proliferative fraction. When calculating the crypt renewal time (i.e. the time taken for a cell to move from the bottom to the top of the crypt) we assume that the cell starts one position up from the bottom of the crypt since the cell velocity is zero at $y = 0$. In practice we expect that the cell dynamics at the bottom of the crypt will be regulated by other factors not considered in our model (e.g. stochastic cell motion and individual stem cell behaviour).

A discussion of the validity of the continuum model hypothesis

In Fig. S7 we present simulation results from a pseudo-steady, two-dimensional crypt. Each cell has two variables: β-catenin concentration, $s_i(t)$, and spatial position, $\mathbf{x}_i$. In the underlying discrete model, each s_i evolves according to Eq. (S5). Cells interact mechanically via a linear force law, hence at each time step of the simulation cell positions are updated using Newton's second law in the overdamped limit (5). Cells divide if their β-catenin concentration exceeds a threshold, s^*, and the axis of cell division is randomly chosen. The data presented in Fig. S7 were obtained by considering a crypt simulation at dynamic equilibrium: each of the r_i and s_i's were

recorded and the cells were subdivided into equally spaced bins of area $\Delta y \Delta s$, allowing a numerical estimation of cell number density in sy space to be calculated. The simulation data are in qualitative agreement with numerical solutions of Eqs. (S9) - (S14), providing an indication that the continuum model represents a reasonable approximation to crypt dynamics. We refer the interested reader to van Leeuwen et al. (5) for further details.

Restriction to one spatial dimension

In a healthy crypt, cell proliferation and differentiation are controlled by chemical gradients that vary along the crypt axis. Accordingly, cell proliferation occurs predominantly at the bottom of the crypt while cell shedding occurs at the top. In a homeostatic crypt, mitochondrial DNA staining experiments indicate that cell motion occurs predominantly along the crypt axis (10, 11); cells that orginate from a common stem cell are observed in narrow ribbands along the crypt axis. Thus in Eq. (S1) only one spatial dimension has been considered.

In (12) we examine the validity of this approximation by comparing numerical results from a two-dimensional simulation of a crypt (similar to Meineke et al. (4)) with the one-dimensional continuum model. A comparison of steady-state velocity fields between the models shows excellent agreement. Moreover, analysis of the continuum model demonstrates that there exists a restricted region of parameter space which permits a homeostatic solution. Subsequently, a corresponding region of parameter space is found for the discrete model. We note that the inherent noise in the two-dimensional simulations resulting from the random positioning of daughter cells upon cell division does not appear to be important at the continuum level of description.

Deriving a form for the cell flux

We have adopted a continuum modelling approach in which cell number density is described as a function of the two independent variables s, the subcellular β-catenin concentration, and y, the cell position along the crypt axis. At each point along the y axis we therefore assume a distribution of cells in s space (see Fig. S1). A valid question to be asked of the modelling methodology is whether or not there are a sufficient number of cells in the crypt such that a continuum framework can accurately capture the evolution of the distributions.

Consider fixed y and assume a population of M_1 cells, each of which has a variable $s_i(t)$ whose deterministic evolution is given by Eq. (S5). Eq. (S5) has a single stable steady-state which we define by $s_0 = s_0(y)$. Subdividing the s axis into boxes of width Δs and defining $M_i(t)$ to be the number of cells in the box centred at s_i, the master equation for the evolution of the stochastic mean in each interior box is given by:

$$\frac{\partial M_i}{\partial t} = T^+_{i-1} M_{i-1} - (T^+_i + T^-_i) M_i + T^-_{i+1} M_{i+1}, \tag{S15}$$

$$\tag{S16}$$

where the T_i^+ and T_i^- denote the transition probabilities of a cell in the i^{th} box moving to the $(i-1)^{st}$ or $(i+1)^{st}$ box, respectively (13). We assume that the transition probabilities have two components: the first represents random hopping between boxes as a result of noise in the system while the second is deterministic and represents changes in β-catenin concentration owing to the underlying β-catenin dynamics given by Eq. (S5).

For the random hopping component of the cell dynamics, we assume the transition probabilities are isotropic and constant, hence

$$T_+ = T_- = \frac{D}{\Delta s^2}, \tag{S17}$$

and Eq. (S15) is given by

$$\frac{\partial M_i}{\partial t} = D\frac{(M_{i-1} - 2M_i + M_{i+1})}{\Delta s^2}. \tag{S18}$$

This equation is of the form of a discretised Laplacian operator, hence the evolution of the stochastic means in time evolve via a diffusive process.

The second term in the transition probabilities originates from the underlying β-catenin dynamics. For each y, Eq. (S5) has the steady-state value $s_0(y)$ with $g(y,s) > 0 \ \forall \ s < s_0(y)$ and $g(y,s) < 0 \ \forall \ s > s_0(y)$ and we assign the transition probabilities as follows:

$$s < s_0(y): \quad T_i^- = 0, \quad T_i^+ = \frac{g(y,s_i)}{\Delta s}, \tag{S19}$$

and

$$s > s_0(y): \quad T_i^- = \frac{g(y,s_i)}{\Delta s}, \quad T_i^+ = 0. \tag{S20}$$

Considering the case when $s < s_0(y)$, Eq. (S15) reduces to

$$\frac{\partial M_i}{\partial t} = \frac{g(y,s_{i-1})M_{i-1} - g(y,s_i)M_i}{\Delta s}, \tag{S21}$$

and making a Taylor expansion of $g(y,s_{i-1})$ about s_i and substituting in Eq. (S21) yields

$$\frac{\partial M_i}{\partial t} = -g\frac{M_i - M_{i-1}}{\Delta s} - M_{i-1}\frac{\partial g}{\partial s}. \tag{S22}$$

Now summing contributions from the two different components, we find that the evolution equations for the stochastic means are given by

$$\frac{\partial M_i}{\partial t} = -g\frac{M_i - M_{i-1}}{\Delta s} - M_{i-1}\frac{\partial g}{\partial s} + D\frac{(M_{i-1} - 2M_i + M_{i+1})}{\Delta s^2}. \tag{S23}$$

Eq. (S23) determines how the stochastic means evolve at each s_i and is a discretised form of the PDE

$$\frac{\partial M}{\partial t} = -\frac{\partial}{\partial s}\left(g(y,s)M - D\frac{\partial M}{\partial s}\right), \tag{S24}$$

with the cell flux of the same form as that derived in Eq. (S7). Hence, we assume that the population density evolves like the stochastic mean of an underlying discrete model.

A model of multiple intestinal crypts

Model development

Integration of Eq. (S9) with respect to s, together with the zero-flux boundary conditions, yields

$$\frac{\partial q}{\partial \tau} = \overbrace{\frac{\partial}{\partial y}\left(D(q)\frac{\partial q}{\partial y}\right)}^{\text{cell movement}} + \overbrace{\rho(1-\frac{q}{K})\int_0^\infty pH(s-s^*)ds}^{\text{source}}, \tag{S25}$$

where $D(q) = \frac{\alpha}{q^2}$ and the source term ensures that cell division is restricted to cells with $s > s^*$. However, the numerical results presented in Figs. 3 and 4 of the Main Text demonstrate that there is a one-to-one relationship between average β-catenin concentration and spatial position along the crypt axis. Motivated by these results we assume that for any value of s^* there is a corresponding crypt position $y^* = y^*(s^*)$ such that cell proliferation occurs in the region $0 < y < y^*$. This assumption allows us to replace the source term in Eq. (S25) by a term that depends on q and y so that

$$\frac{\partial q}{\partial \tau} = \overbrace{\frac{\partial}{\partial y}\left(D(q)\frac{\partial q}{\partial y}\right)}^{\text{cell movement}} + \overbrace{\rho q(1-\frac{q}{K})H(y^*-y)}^{\text{source}}, \tag{S26}$$

and the PDE for q is independent of s. We note that the parameter y^* can be related to the β-catenin dynamics by considering numerical solutions of the model presented in the previous section as necessary.

As illustrated in Fig. 5 of the Main Text, we now consider a spatial domain $y \in [-NL, NL]$ with the crypt bottoms and tops positioned at $\{..,-2L,0,2L,..\}$ and $\{..,-L,L,..\}$, respectively. The independent variable y now represents arc length along the chain of connected crypts and the source term in Eq. (S26) is generalised to be a periodic binary function which models the localisation of cell proliferation to the bottom of each crypt.

In the single crypt model cell shedding was incorporated via boundary condition (6) is the Main Text, which states that cells at the top of the crypt experience zero force from above (i.e. we implicitly assumed that the removal rate maintained the cell number density at $y = L$ at the constant value $\frac{1}{l}$). When considering interactions between cells in neighbouring crypts, we can no longer model cell removal at the top of each crypt through a Dirichlet boundary condition. Instead we introduce a cell shedding term with the spatial form depicted in Fig. 5 (dashed line) and Eq. (S26) is modified such that

$$\frac{\partial q(y,\tau)}{\partial \tau} = \frac{\partial}{\partial y}\left(D(q)\frac{\partial q}{\partial y}\right) + \rho f(y,y^*)q(1-\frac{q}{K}) - \overbrace{\delta q g(y,y_D)}^{\text{Shedding}}, \tag{S27}$$

where δ is the linear shedding rate, and $g(y,y_D)$ and $f(y,y^*)$ are periodic, binary functions which model cell shedding and birth, respectively (see Fig. 5 of the Main Text).

We close Eq. (S27) by imposing periodic boundary and initial conditions of the form

$$q(-NL,\tau) = q(NL,\tau), \tag{S28}$$

$$\frac{\partial q}{\partial y}_{y=-NL} = \frac{\partial q}{\partial y}_{y=NL}, \tag{S29}$$

$$q(y,0) = q_0, \tag{S30}$$

with N chosen to be large enough (e.g. $N = 5$ in the examples shown below) such that boundary effects can be neglected over time-scales of interest. When computing numerical solutions of Eqs. (S27) - (S30), we use a regular mesh with N_y nodes to discretise the domain $-NL \leq y \leq NL$. At each time step, the spatial partial derivatives that appear in Eq. (S27) are approximated using finite differences. The method of lines is then used to solve the resulting system of nonlinear ODEs.

Numerical Results

In order to describe cell shedding and proliferation where there are multiple crypts we have introduced three parameters: y^*, δ and y_D. The parameter y^* is the crypt height below which cell division occurs and can be related to the β-catenin threshold using the model results (Eqs. (2) - (8)) presented in Fig. 4. The rate of cell shedding at the top of the crypts, δ, is fixed such that the total rate of shedding is equal to the experimentally known total rate of cell production at steady-state (e.g. 250 cells per day per crypt in small intestinal crypts (9)). The parameter y_D bounds the spatial region over which cell shedding occurs which we assume to be only at the very top of each crypt (e.g. for the crypt centred at $y = 0$ shedding occurs in the region $y_D < |y| < L$).

In Fig. S8 numerical results depicting the steady-state solution profiles of the multiple crypt model (Eqs. (S27) - (S30)) are presented; a population of normal cells has evolved to dynamic equilibrium such that there is a balance between the net rates of cell shedding and proliferation at the top and bottom of each crypt, respectively. The cell velocities (which depend on density gradients) are zero at the bottom of each crypt, increase in magnitude along the crypt axes (e.g. $v(y) < 0$ for $y \in [-L, 0]$, as cells move up the left-hand crypt), and are zero again at the top of each crypt. These results indicate that the behaviour of each individual crypt in the multiple crypt model is in broad agreement with previous models of single crypts (e.g. cell proliferation at the bottom of each crypt resulting in cells moving up each crypt and being shed at the top).

Introducing a second cell population

Model development

We now consider populations of normal and mutated cells with number densities $q_1(y,\tau)$ and $q_2(y,\tau)$, respectively, whose shedding rates (δ_1 and δ_2) and division

thresholds (y_{C1} and y_{C2}) are different. The total cell density is defined to be $q(y,\tau) = q_1(y,\tau) + q_2(y,\tau)$. Applying the principle of conservation of cell number to each cell population we obtain

$$\frac{\partial q_i}{\partial \tau} + \frac{\partial J_{yi}}{\partial y} = \rho f(y, y_{Ci}) q_i (1 - \frac{q}{K}) - \delta_i q_i g(y, y_{Di}); \quad i = 1, 2, \tag{S31}$$

where J_{yi} are the cell fluxes. As in the previous section we assume that the total cell flux (J_y) is given by

$$J_y = J_{y1} + J_{y2} = -\frac{\alpha}{q^2}\frac{\partial q}{\partial y} = -D(q)\frac{\partial q}{\partial y}. \tag{S32}$$

For simplicity we suppose that the individual cell fluxes are weighted according to their relative cell number density so that

$$J_{yi} = -\frac{q_i}{q}\frac{\alpha}{q^2}\frac{\partial q}{\partial y}; \quad i = 1, 2. \tag{S33}$$

We note that the cell fluxes J_{yi} are similar in form to those considered in a model of avascular tumour growth devised by (14). The main difference between our model and the earlier work is that they assume $D(q)$ to be constant and hence recover linear diffusion, whereas because we assume that the cells are connected by overdamped linear springs $D(q) = \frac{\alpha}{q^2}$.

In order to examine the behaviour of a small population of 'mutant' cells that are initially centred around some region of the crypt $y = y_0$, we define $q_{ss}(y)$ to be the steady-state solution in the case of a single normal cell population and choose as initial conditions

$$q_2(y, 0) = q_{ss}(y) e^{\frac{-(y-y_0)^2}{2\sigma^2}} \tag{S34}$$

and

$$q_1(y, 0) = q_{ss}(y) - q_2(y, 0), \tag{S35}$$

where σ is a lengthscale characterising the initial size of the patch of introduced mutant cells. We close Eqs. (S31)-(S35) by imposing periodic boundary conditions of the form

$$q_i(-NL, \tau) = q_i(NL, \tau), \tag{S36}$$

$$\frac{\partial q_i}{\partial y}_{y=-NL} = \frac{\partial q_i}{\partial y}_{y=NL}; \quad i = 1, 2. \tag{S37}$$

A schematic illustration of the simulation results presented in Fig. 6 of the Main Text is presented in Fig. S9: (a) a small patch of mutated cells is initially placed in the centre of the homeostatic central crypt (i.e. at $y = 0$). Numerical simulations are performed using these initial data for different parameter values; (b) the mutant cell population has a neutral mutation; (c) the mutant cells proliferate throughout the crypt and (d) the mutant cells proliferate throughout the crypt and have a reduced shedding rate. This combination of parameter changes results in the mutant cells migrating into neighbouring crypts.

References

1. Dyson, J., E. Sanchez, R. Villella-Bressan, and G. Webb, 2007. An age and spatially structured model of tumor invasion with haptotaxis. *Discrete and continuous dynamical systems* 8:45.

2. Webb, G., 2008. Population models structured by age, size, and spatial position. *Lecture notes in mathematics* 1936:1.

3. Murray, P. J., C. M. Edwards, M. J. Tindall, and P. K. Maini, 2009. From a discrete to a continuum model of cell dynamics in one dimension. *Physical Review E* 80 (3):031912–1–031912–10.

4. Meineke, F., C. Potten, and M. Loeffler, 2001. Cell migration and organization in the intestinal crypt using a lattice-free model. *Cell Prolif.* 34:253–266.

5. van Leeuwen, I., G. Mirams, A. Walter, A. Fletcher, P. Murray, J. Osborne, S. Varma, S. Young, J. Cooper, B. Doyle, J. Pitt-Francis, L. Momtahan, P. Pathmanathan, J. Whiteley, S. Chapman, D. Gavaghan, O. Jensen, J. King, P. Maini, S. Waters, and H. Byrne, 2009. An integrative computational model for intestinal tissue renewal. *Cell Prolif.* 42 (5).

6. Lee, E., A. Salic, R. Kruger, R. Heinrich, and M. Kirschner, 2003. The roles of APC and Axin derived from experimental and theoretical analysis of the Wnt pathway. *PLoS Biol* 1:116–132.

7. Mirams, G. R., H. M. Byrne, and J. R. King, 2010. A multiple timescale analysis of a mathematical model of the Wnt/β-catenin signalling pathway. *J. Math. Biol.* 60:131–160.

8. Cho, K., S. Baek, and M. Sung, 2006. Wnt pathway mutations selected by optimal β-catenin signaling for tumorigenesis. *FEBS letters* 580:3665–3670.

9. Potten, C., and M. Loeffler, 1990. Stem cells: attributes, cycles, spirals, pitfalls and uncertainties. Lessons for and from the crypt. *Development* 110:1001–1020.

10. Taylor, R., M. Barron, G. Borthwick, A. Gospel, P. Chinnery, D. Samuels, G. Taylor, S. Plusa, S. Needham, L. Greaves, et al., 2003. Mitochondrial DNA mutations in human colonic crypt stem cells. *Journal of Clinical Investigation* 112:1351–1360.

11. McDonald, S., S. Preston, L. Greaves, S. Leedham, M. Lovell, J. Jankowski, D. Turnbull, and N. Wright, 2006. Clonal expansion in the human gut: mitochondrial DNA mutations show us the way. *Cell Cycle* 5:808–811.

12. Murray, P. J., A. Walter, C. M. Edwards, M. J. Tindall, and P. K. Maini, 2010. Modelling cell dynamics in the crypt. *In preparation* .

13. Erban, R., S. Chapman, and P. Maini, 2007. A practical guide to stochastic simulations of reaction–diffusion processes `http://arxiv.org/abs/0704.1908`.

14. Sherratt, J., and M. Chaplain, 2001. A new mathematical model for avascular tumour growth. *J. Math. Biol.* 43:291–312.

Table S1: Comparison of murine intestinal crypt data taken from Potten and Loeffler (9) with results from the continuum model at dynamic equilibrium. $N_s = 50$, $N_y = 15$, $\lambda = 3$, $D_s = 25$, $s^* = 100$, $\rho = 0.1$, $\alpha = 35$, $K = 2$.

Quantity	Continuum model	Numerical estimate	Experimental data
Cell number	$N_x \int_0^L \int_0^\infty p ds dy$	288 cells	250-300 cells
Renewal time	$\int_1^L \frac{q^3}{\alpha} (\frac{\partial q}{\partial y})^{-1} dy$	2.4 days	2-3 days
Proliferative fraction	$\frac{\int_0^L \int_0^{s^*} p ds dy}{\int_0^L \int_0^\infty p ds dy}$	0.6	0.67

Figure Legends

Fig. S1.

A schematic illustration of the crypt continuum model. In the discrete model (left), y is the spatial coordinate along the crypt axis, L denotes the crypt height and α the resting spring length. Unit length is chosen to be a cell diameter, l. Each cell is defined by the coordinate pair (y_i, s_i). In the continuum model, we assume that there is a distribution of β-catenin for each volume element along the crypt axis, Δy. Every volume element (e.g. the hatched region) has an associated cell number density, $p(y, s)$, and on the right-hand side, a schematic of how $p(y, s)$, varies with y and s is depicted. In this schematic cells have high and low β-catenin concentrations at the bottom ($y = 0$) and top ($y = L$) of the crypt, respectively.

Fig. S2.

The steady-state of Eq. (S6) is plotted against y for $W(y)$ given by Eq. (4) of the main text.

Fig. S3.

A plot of average β-catenin concentrations along the crypt axis for wild-type (starred line), m7 (solid line), m8 (dashed line) and m9 (dotted line) parameter sets presented in Table **??**. Eqs. (S9) - (S14) were solved numerically until a dynamic equilibrium was reached. Plots shown at $\tau = 40$ hours with parameters as in Tables **??** and **??**. $\bar{s}$ was then numerically calculated using Eq. (**??**).

Fig. S4.

Additional numerical results from the single crypt continuum model (Eqs. (S9) - (S14)) at dynamic equilibrium. Here the β-catenin production rate is increased by a factor of two, ($a = 50$.) Other details as in Fig. 2 of the Main Text.

Fig. S5.

Additional numerical results from the single crypt continuum model (Eqs. (S9) - (S14)) at dynamic equilibrium. Here $T_C = 10$. Other details as in Fig. 2 of the Main Text.

Fig. S6.

Additional numerical results from the single crypt continuum model (Eqs. (S9) - (S14)) at dynamic equilibrium. Here $D_s = 12$. Other details as in Fig. 2 of the Main Text.

Fig. S7.

Simulation results from a two-dimensional discrete crypt model. (a) A plot of the cell distribution. (b) Cell density plotted against y and s. Densities calculated by binning simulation data into regular equally-spaced bins of area $\Delta y \Delta s$. Here $\Delta y = 2$ and $\Delta s = 10$.

Fig. S8.

Cell density (solid line) and velocity (dashed line) fields are plotted against spatial coordinate, y. The proliferation (f) and shedding (g) functions are denoted by the dot-dashed lines, respectively. Eqs. (S27) - (S30) were solved numerically using the finite difference method. In this plot $\alpha = 35$, $y^* = 0.6L$, $y_D = 0.15L$, $\rho = 0.1$, $\delta = 0.09$, $N = 5$, $L = 16$, $K = 2$ and $N_y = 281$.

Fig. S9.

A schematic illustration of the biological interpretation of the numerical results presented in Fig. 5: (a) initial conditions – a small mutant population (shaded cells) is introduced into the bottom of the central crypt; (b) a neutral mutation: mutated cells have the same parameters as the normal cells. As the mutated cell population is introduced at the bottom it pushes the normal cells out of the central crypt; (c) a cell proliferation mutation – the mutant cells proliferate throughout the crypt resulting in an increased cell density in the mutant crypt; (d) a cell proliferation and shedding mutation allows the mutant population to invade into the neighbouring crypts.

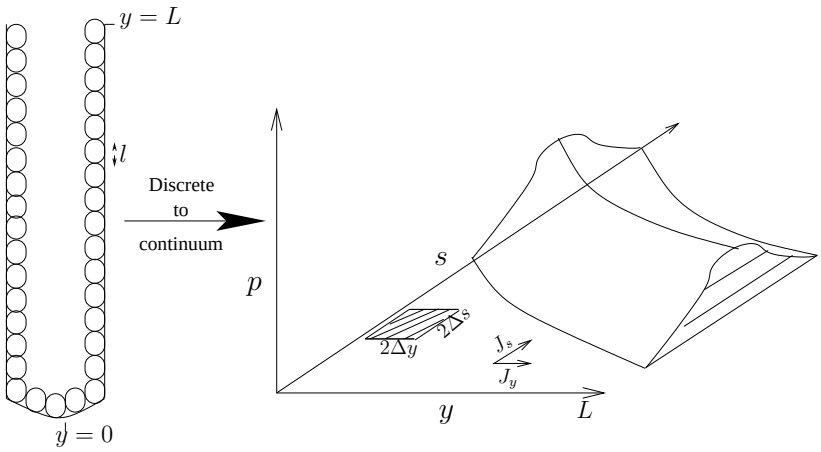

Figure S1:

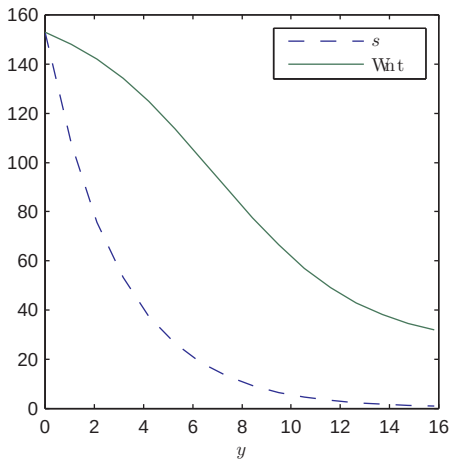

Figure S2:

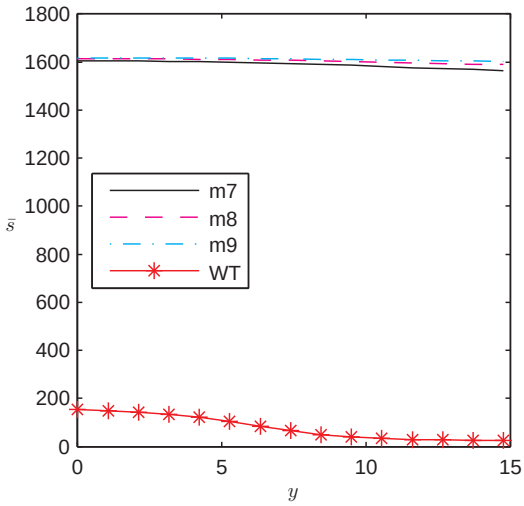
1800
1600
1400
1200
1000
800
600
400
200
0
0
5
10
15
s_1
y
m7
m8
m9
WT

Figure S3:

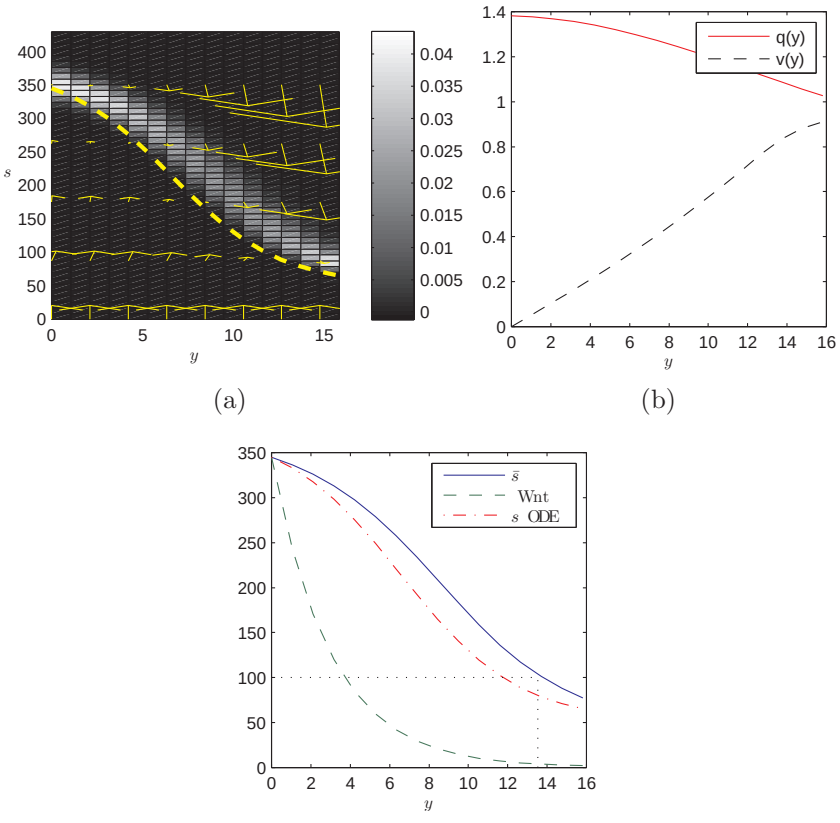

(a) (b)

(c)

Figure S4:

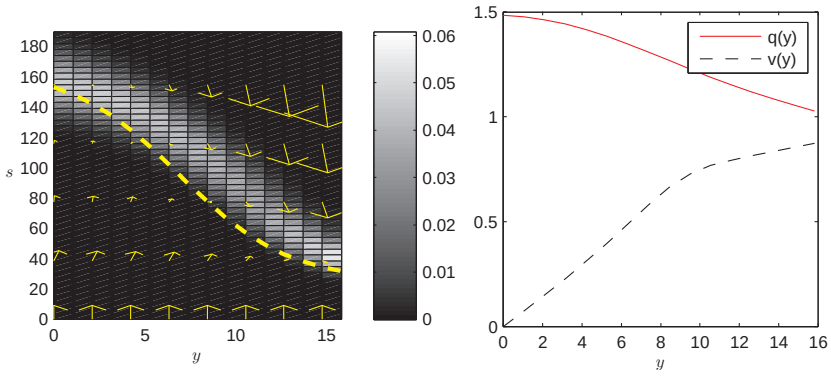

(a) (b)

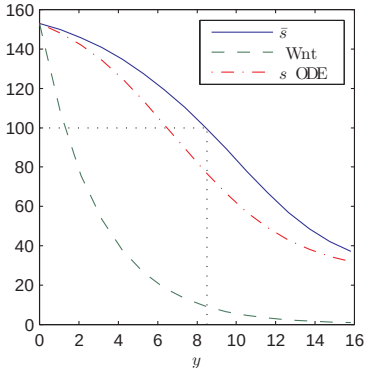

(c)

Figure S5:

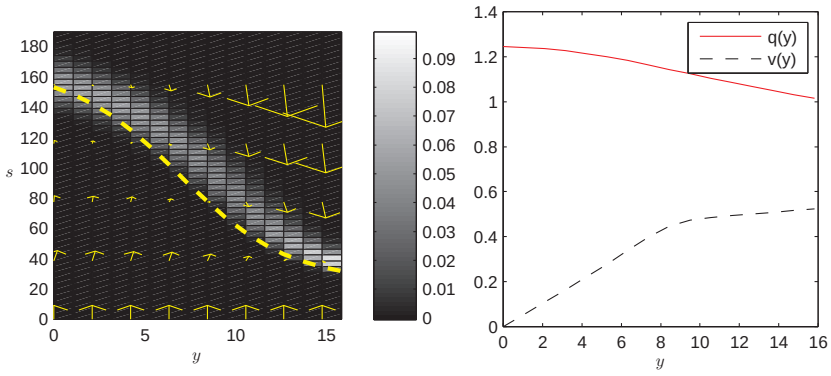

(a) (b)

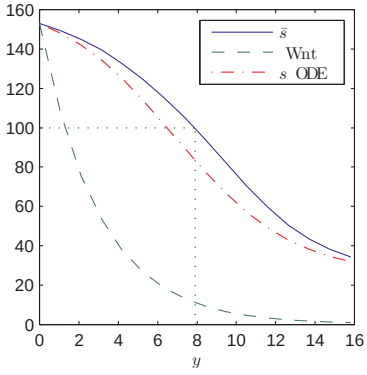

(c)

Figure S6:

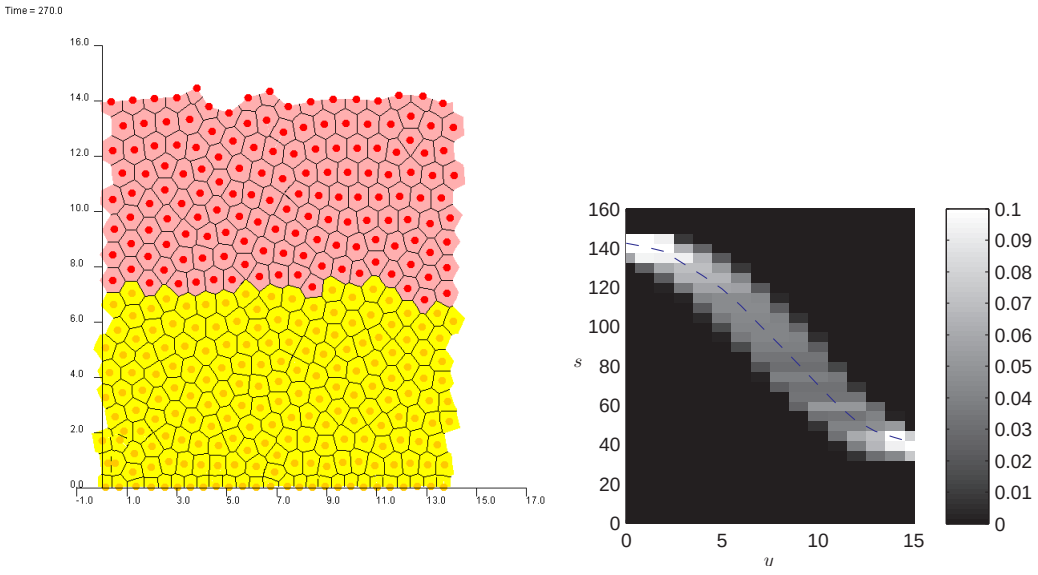
Time = 270.0
16.0
14.0
12.0
10.0
8.0
6.0
4.0
2.0
0.0
-1.0
1.0
3.0
5.0
7.0
9.0
11.0
13.0
15.0
17.0
160
140
120
100
80
60
40
20
0
s
0
5
10
15
u
0.1
0.09
0.08
0.07
0.06
0.05
0.04
0.03
0.02
0.01
0

Figure S7:

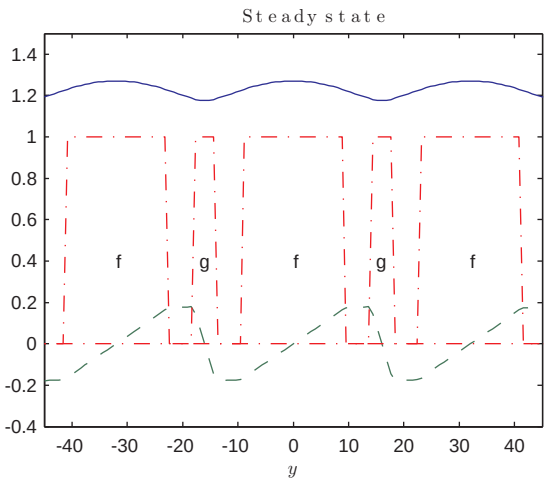
Steady state
1.4
1.2
1
0.8
0.6
0.4
0.2
0
-0.2
-0.4
f
g
f
g
f
-40
-30
-20
-10
0
10
20
30
40
y

Figure S8:

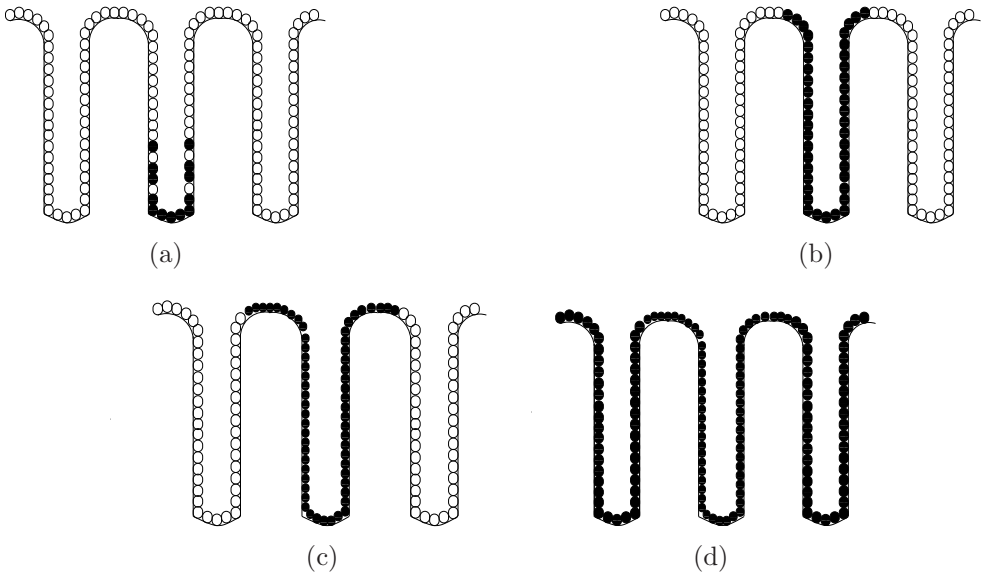

Figure S9: